



## Predicting Nonlinear Site Response Using Spectral Acceleration Vs PGV/Vs30: A Case History Using the Volvi-Test Site

PHILIPPE GUÉGUEN<sup>1</sup>

**Abstract**—In this study, we analyze the efficiency of the ratio between particle velocity and shear wave velocity as a strain proxy for evaluating the nonlinear seismic response of sediments. The in situ stress–strain relationships are derived from accelerometric vertical array recordings at the TST site in Volvi (Thessaloniki, Greece). First, the shear wave velocity between two successive sensors was computed by seismic interferometry and strain was computed as the velocity ratio or the relative displacement between sensors. The shear-wave velocity profile and in situ shear modulus degradation curve with strain were compared with previous studies performed at the TST site. Finally, the stress–strain relationships were derived from data recorded at the surface by extending the strain proxy and stress values to the ratio between peak ground velocity and the  $Vs30$  parameter used for site classification, i.e. without requiring the accelerometric vertical array. Our model captures the in situ nonlinear response of the site, without consideration of azimuth or distance of the earthquakes. In conclusion, the acceleration (stress) values, based on the accelerometric response spectra instead of peak ground acceleration compared with the deformation (strain) proxy, provide an effective model of the in situ nonlinear response, providing information that can be integrated into ground motion prediction equations.

**Key words:** Nonlinear response, sediments, seismic interferometry, Volvi test site.

### 1. Introduction

Low-velocity soft sediments are generally considered to be a critical component of seismic hazard, amplifying the seismic ground motion and partly controlling the spatial variability of building damage. On the other hand, it is also commonly assumed that unconsolidated sediments tend to respond in a nonlinear manner, which can serve to modify seismic

ground motion (e.g., FIELD *et al.* 1997; BONILLA *et al.* 2005; ROUMELIOTI and BERESNEV 2003). As a result, new equations are being developed to introduce non-linearity and to consider its effects on the standard deviation of seismic ground motion predictions according to specific parameters, such as magnitude and distance (ABRAHAMSON *et al.* 2014; BOORE *et al.* 2014), which always require geotechnical in situ characterization of the site and a way of characterizing the nonlinear response in the data. The nonlinear response of sediments is usually considered as the result of the degradation of the shear modulus  $G$  and the increase in damping  $\zeta$  as the soil shear strain  $\gamma$  increases. Consequently nonlinear soil behaviour tends to modify site response in a frequency dependent way. These modifications can include a decrease of the high frequency amplification due to increased damping (e.g., DIMITRIU *et al.* 2001; FRANKEL *et al.* 2002; PAVLENKO and IRIKURA 2002; RUBINSTEIN and BEROZA 2004, 2005; ASSIMAKI *et al.* 2008; BONILLA *et al.* 2011), a shift of energy to lower frequencies due to decrease in shear wave velocity that can actually amplify site response relative to linear or low strain motions (e.g., BONILLA *et al.* 2005; WU *et al.* 2009), and when excess pore pressure is generated, cyclic dilatancy can occur, increasing very high frequency site response (e.g., BONILLA *et al.* 2005).

Nonlinear site characterization is required to estimate the seismic ground motion variability observed in data and influence the uncertainties of prediction equations. Such estimates are based on the characterization of shear wave velocity in the upper sediment layers and the testing of soil samples in the laboratory by cyclic and/or dynamic tests. Differences exist between laboratory results and in situ observations due to the difficulties among others of

<sup>1</sup> ISTerre, CNRS/IFSTTAR, Université Grenoble–Alpes, BP 53, 38041 Grenoble cedex 9, France. E-mail: philippe.gueguen@ujf-grenoble.fr

reproducing stress–strain conditions and of separating nonlinear effects from site amplification effects, including for example 2D/3D geometrical effects (FRANKEL *et al.* 2002; SLEEP 2010; GÉLIS and BONILLA 2012). Moreover, it is difficult to generalize laboratory tests to all recording sites and all depths where nonlinearity can be expected which may be located not only at the surface. However, nonlinear response is directly related to the variation of shear (modulus and strain) and one solution consists in assessing the shear-wave velocity ( $V_s$ ) of soil during strong ground strain. For site-specific analysis, improving  $V_s$  characterization directly from in situ data is helpful in reducing the level of uncertainty in ground motion prediction as discussed in KIM *et al.* (2015).

Specialized arrays with borehole accelerometers are used to resolve the scattering vs nonlinearity problem (FRANKEL 1999). Methods exist to assess  $V_s$  along a vertical borehole array based on cross correlation (ZEGHAL *et al.* 1995; PAVLENKO and IRIKURA 2003; RUBINSTEIN and BEROZA 2004, 2005) or seismic interferometry by deconvolution (SAWAZAKI *et al.* 2009; NAKATA and SNIEDER 2011, 2012; MEHTA *et al.* 2007; CHANDRA *et al.* 2015). The nonlinear behavior of soil can then be given by the stress–strain relationship observed on site or by the  $G/G_{\max} - \gamma$  curves, with  $G_{\max}$  corresponding to the elastic shear modulus. There is a relationship between  $G$  and  $V_s$ , i.e.  $V_s = (G/\rho)^{1/2}$ , and CHANDRA *et al.* (2015) showed that the variation of  $V_s$  tracked by seismic interferometry applied to an accelerometric vertical array is an accurate solution for observing nonlinearity related to seismic ground motion amplitude. Finally, considering each earthquake recording as a single in situ cyclic test, the vertical variation of shear strain can be simultaneously computed as the relative horizontal displacement along the borehole. This means having a vertical geotechnical array of accelerometers, which is not available everywhere. However, RATHJE *et al.* (2004) proposed considering the ratio of peak ground velocity (PGV) and shear wave velocity  $V_s$  (i.e.  $PGV/V_s$ ) as a strain proxy. IDRIS (2011) recently proposed a generalization of this relationship that considers peak-ground acceleration (PGA) vs  $PGV/V_s30$  as the in situ stress–strain relationship. In this case,  $V_s30$  is the average shear wave velocity in the upper 30 m layers conventionally used in

earthquake engineering as a site classification parameter and considered as a convenient input in ground motion prediction equations. In this case, it is considered that the nonlinearity appears essentially in the uppermost layers even though CHANDRA *et al.* (2015) showed that beyond 30 m depth, soils may have nonlinear behavior.

DE MARTIN *et al.* (2012) and CHANDRA *et al.* (2015) tested the efficiency of  $PGV/V_s30$  as a strain proxy but additional tests must be conducted in order to analyze the magnitude or distance dependency of the nonlinear proxy to be included in ground motion prediction equations. This paper therefore concentrates on the accelerometric vertical array at the TST Volvi site (Greece). After describing the test site and data, the data processing and seismic interferometry by deconvolution methods are presented and the results are compared with the shear velocity reference profile derived from geophysical methods. Then, the efficiency of the strain proxy is analyzed jointly with the in situ stress–strain relationship observed and finally the in situ proxy of nonlinear response for the site-specific prediction of ground motion is discussed in the last section.

## 2. Site Characterization of the Volvi Test-Site Basin

Data were recorded at the Volvi test site (Greece), located in the sedimentary basin around 20 km to the north of Thessaloniki (Fig. 1a). The geotechnical and geophysical properties of the sediments (Fig. 1c) have been studied by a number of investigators, providing reliable 2D and/or 3D soil models for seismic ground motion modeling (e.g., JONGMANS *et al.* 1998; RAPTAKIS *et al.* 2000, 2005; MANAKOU *et al.* 2010). RAPTAKIS and MAKRA (2015) provides a synthesis of the variability of the soil profile compiled from all the studies. A geotechnical borehole has been drilled in the center of the Volvi basin (Fig. 1c) and instrumented with a permanent vertical three-component accelerometric array (TST borehole). Interpretation of the surveys in terms of shear and body wave profiles yields  $V_s$  and  $V_p$  values ranging from 165 to 870 m/s and from 325 to 2700 m/s, respectively, from the surface to the bedrock (RAPTAKIS *et al.* 2000). The soil is mainly silty-

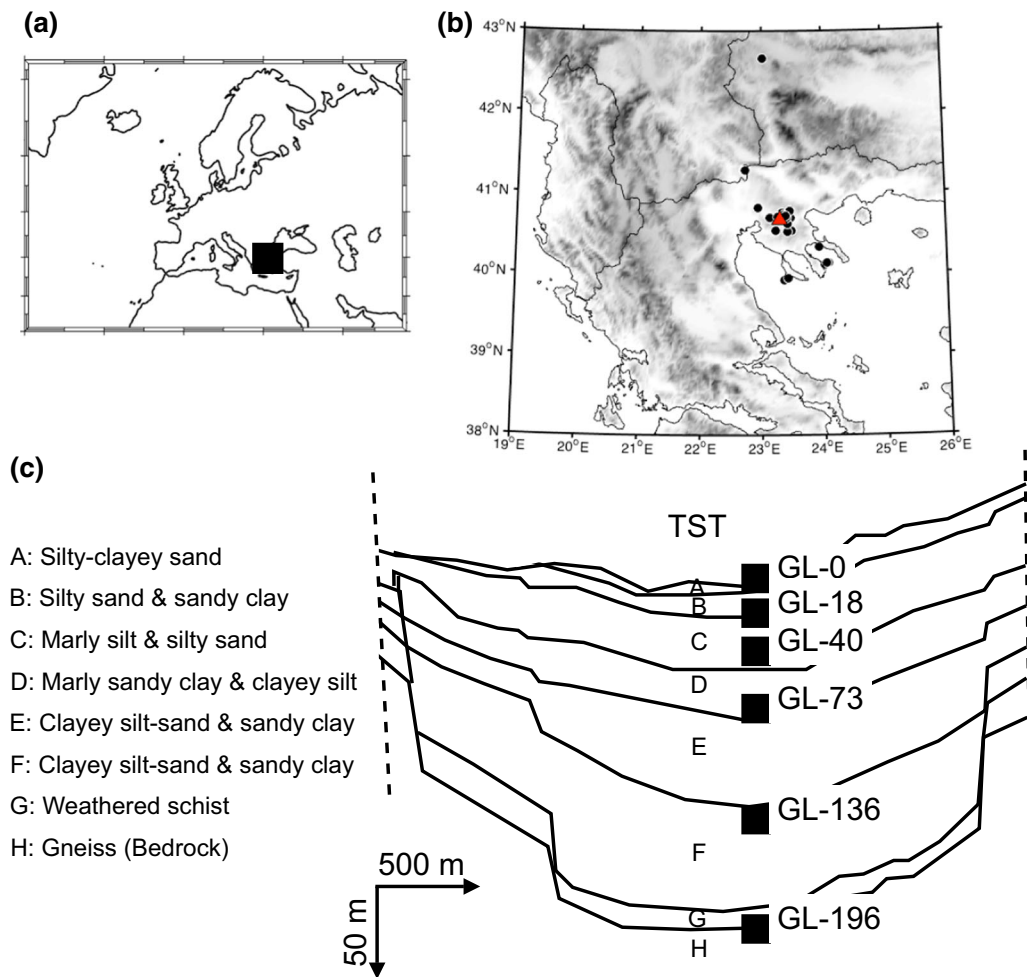


Figure 1

**a** Location of the Volvi test site (Greece). **b** Location of the earthquakes used in this study (triangles TST, circles epicenters). **c** Cross-section of the Volvi basin centered on the TST borehole (squares accelerometers) (according to RAPTAKIS and MAKRA 2015)

clayey sand and sand in the sedimentary part; the bedrock is gneiss, lying at a depth of about 190 m. The TST site can be considered as an equivalent 2D shaped basin characterized by a horizontally layered, flat soil column. The bedrock is relatively stiff with  $V_s$  equal to 2300 m/s. As a result, strong seismic ground motion amplification has been reported at the TST (MANAKOU *et al.* 2010), with a resonance frequency of 0.6–0.7 Hz in the center of the basin, based on accelerometric data analysis and ambient vibration measurements.

The shallow-depth vertical array (<http://euroseisdb.civil.auth.gr/>, PITILAKIS *et al.* 2013) consists of six 3-component accelerometers (Fig. 1c)

located on the surface (GL-0), and at depths of 18.7 m (GL-18), 40 m (GL-40), 73.1 m (GL-73), 136 m (GL-136) and 196 m (GL-196) (GL means Ground Level). Note that the deepest sensor is located at the interface between sediment and bedrock. All the sensors are connected to the same digital acquisition system to ensure perfect synchronization. A GPS receiver controls absolute time. Raw data are triggered, corrected in terms of baseline offset and the horizontal components of the recordings are rotated with respect to the north–south and east–west directions. Delays were experienced during sensor installation and gaps in data continuity are observed. Consequently, we only considered data that allow the

estimation of shear wave velocity between two sensors, i.e. recorded at least by the GL-0 sensor and another one. In total, 24 events were used in this study, recorded between 2008 and 2014 (Fig. 1b). Magnitudes range from 2.1 to 5.8, with epicentral distances of between 4 and 220 km, corresponding to a PGA between 0.78 and 97 cm/s<sup>2</sup> and 0.93 and 101 cm/s<sup>2</sup> in the north–south and east–west directions, respectively.

### 3. Shear Wave Velocity Assessment

The premise of seismic interferometry applied to a vertical array was given by ZEGHAL *et al.* (1995). It consists in cross-correlating data recorded by two different sensors to extract the impulse response or Green's function between them (e.g., LOBKIS and WEAVER 2001; DERODE *et al.* 2003; SCHUSTER *et al.* 2004; SNIEDER 2004; WAPENAAR 2004; SHAPIRO *et al.* 2005; SNIEDER *et al.* 2006; WAPENAAR *et al.* 2010). Recently, SNIEDER and SAFAK (2006) proposed to use deconvolution instead cross-correlation as an interferometric tool; this has since been applied successfully to geotechnical boreholes (MEHTA *et al.* 2007; NAKATA and SNIEDER 2011, 2012; PECH *et al.* 2012; CHANDRA *et al.* 2015). The waveforms recorded by the sensors in different positions along the vertical array are deconvoluted with the recording at the top and the upward and downward waves along the array are obtained. The result provides an equivalent pulse travelling along the array and corresponds to the 1D impulse response of the system. The time delay of the pulse between the two sensors corresponds to the velocity of wave propagating in the medium. In this study, deconvolution is computed using the water level regularization technique proposed by CLAYTON and WIGGINS (1976) and Eqs. 1–5 are derived from this paper. The general model considered assumes system output to be:

$$o(t) = i(t) \otimes h(t) + n(t) \quad (1)$$

where  $o(t)$  is the output signal corresponding to system motion recorded at the ground surface,  $i(t)$  is the seismic input motion at the bottom or intermediary depth of the sedimentary layer,  $h(t)$  is the impulse response of the soil column between input and output recording positions,  $n(t)$  is the noise function

affecting the signal and  $\otimes$  denotes convolution. The estimated impulse response of the borehole is obtained as the inverse Fourier transform of the spectrum of output  $O(\omega)$  divided by the input signal  $I(\omega)$ :

$$\tilde{H}(\omega) = \frac{O(\omega)}{\tilde{I}(\omega)} = \frac{I(\omega)\tilde{I}^*(\omega)}{|\tilde{I}(\omega)|^2}H(\omega) + \frac{\tilde{I}^*(\omega)}{|\tilde{I}(\omega)|^2}N(\omega) \quad (2)$$

where uppercase indicates the Fourier domain,  $\omega$  is the circular frequency,  $*$  denotes conjugation and  $\sim$  are estimated functions. In order to establish a minimum amplitude level for the input to limit the noise term, the minimum input amplitude is named waterlevel, expressed as a fraction of the input. Assuming  $k$  to be the waterlevel parameter ( $0 \leq k \leq 1$ ) and considering the maximum spectral amplitude of the input signal  $|I(\omega)_{\max}|$ ,  $H(\omega)$  becomes:

$$\tilde{H}(\omega) = \frac{I(\omega)\tilde{I}^*(\omega)H(\omega) + N(\omega)\tilde{I}^*(\omega)}{\max\left\{|\tilde{I}(\omega)|^2, \left(K|I(\omega)_{\max}|\right)^2\right\}} \quad (3)$$

The deconvolution process will be stable if the factor

$$\frac{I(\omega)\tilde{I}^*(\omega)}{\max\left\{|\tilde{I}(\omega)|^2, \left(K|I(\omega)_{\max}|\right)^2\right\}} \quad (4)$$

remains stable as a function of frequency. Assuming a good signal-to-noise ratio at ground level, the transfer function of the system is computed as follows:

$$H(\omega) = \frac{O(\omega)}{\max\left\{I(\omega); \left(k|I(\omega)|\frac{I(\omega)}{|I(\omega)|}\right)_{\max}\right\}} \quad (5)$$

After testing the slight influence of the  $k$  value, it was set at 10 % of the average spectral power.

Before deconvolution, the mean and trend of the data were removed and a two-order Butterworth filter was applied between 0.5 and 15 Hz to ensure accurate estimation of travel time. After deconvolution, the inverse Fourier Transform of  $H(\omega)_{i-0m}$  (Eq. 5) was computed to obtain the impulse response of the column between sensors  $GL-i$  and  $GL-0$ . The impulse response was resampled ten times using a

polyphase implementation technique to improve the accuracy of travel time picking. Finally, wave velocity was computed by dividing the distance between  $GL-i$  and  $GL-0$  by the time delay of the pulse, which corresponds to the wave propagation generated by earthquakes along the borehole. Since the soil column is considered as a resonant system with a shear deformation (NAKATA and SNIEDER 2012), shear wave velocity  $V_s$  was computed from the pulse travel time delay based on accelerometric data recorded in the horizontal direction. In the same manner, compressive wave velocity  $V_p$  can be computed based on compressive strain along the borehole, i.e. using accelerometric data recorded in the vertical direction.

Figure 2 shows an example of the travel time delay of the pulse propagating along the vertical array. In our case, the travel time between each sensor was extracted from the causal propagation by picking the time delay between two successive pulses in the negative part.

Figure 2a shows the horizontal pulse computed using east–west sensor recordings and Fig. 2b shows the vertical pulse computed using vertical recordings. A smaller time delay is observed on the vertical component, resulting from the faster propagation of compressive strain along the borehole. In the uppermost layers, the mixture of upward and downward waves at  $GL-18$  m, due to the high value of  $V_p$  compared with the short distance between  $GL-0$  and  $GL-18$ , does not allow separation of the waves. CHANDRA *et al.* (2015) have already reported this limitation of the time delay assessment in the upper layers in the case of two sensors close to one another. In our case, this is mainly true for P wave velocity, since  $V_s$  in the upper layers of the TST site is very low (RAPTAKIS *et al.*, 2000). The signal-to-noise (S/N) ratio of the pulse changes with depth along the borehole. At  $GL-196$ , we observe (Fig. 2) a low S/N ratio that introduces uncertain picking of the pulse time delay, increasing the variability of the velocity assessment.

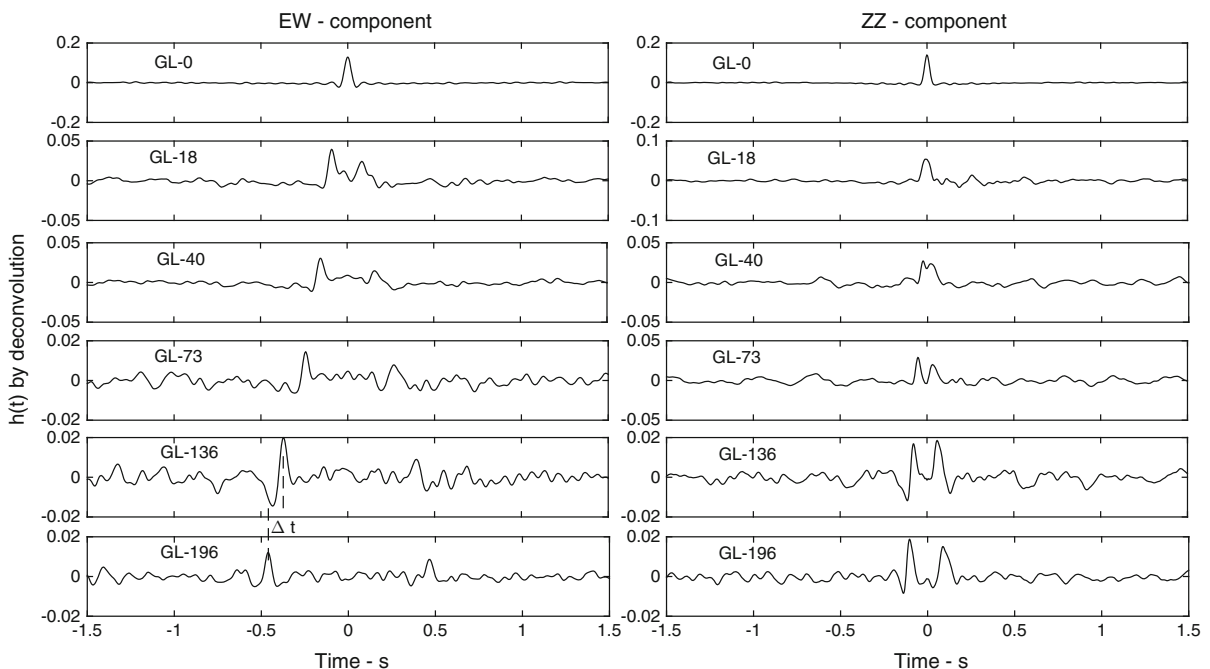


Figure 2

Pulse travel time along the TST borehole along the east–west **a** and vertical **b** directions computed by deconvolution with  $GL-0$  m recordings. Example given for a magnitude 3.5 earthquake

Figure 3 shows the  $V_p$  and  $V_s$  values deep down along the borehole profile computed using seismic interferometry by deconvolution. North–south and east–west directions are considered separately. We compared our results with the soil profile given by RAPTAKIS *et al.* (2000) considered as a reference for the TST site. Furthermore, we superimposed the smoothed velocity profiles derived from Raptakis' reference profile by averaging the velocity between the sensor positions. All the earthquakes were used, regardless of azimuth, magnitude and distance characteristics that may affect the vertical propagation of body waves. The results (Fig. 3) are quite stable, with small standard deviations changing as depth along the borehole increases. The  $V_p$  value in the uppermost layers is less clear because of the mixture of upward and downward waves (Fig. 2). Between GL-136 and GL196, the  $V_s$  profile is less stable in the EW direction related to the S/N ratio. In general, a good fit is observed with the smoothed Raptakis model for  $V_s$  and  $V_p$  at greater depth, with  $V_s$  values in the most superficial layers higher than in the reference model. This paper does not aim to conclude on the most

accurate values of  $V_s$  and  $V_p$ . However, RAPTAKIS and MAKRA (2015) compiled all the geophysical surveys performed in the Volvi basin, based on invasive and non-invasive geophysical methods. They concluded non-negligible variability of the velocity profile (about 20 % but varying in depth). This variability may introduce uncertainties for the site condition classification based on the average 30 m-depth shear wave velocity ( $V_{s30}$ ) which is used in earthquake engineering. In this study, the variability of  $V_s$  may result from the complex geomorphological characteristics of the basin related to the azimuth of the earthquake. However,  $V_s$  and  $V_p$  profiles using seismic interferometry have a smaller standard deviation (below 5 %) than the results extracted from non-invasive methods. For these methods, dispersion curves are inverted in term of velocity and interface depths and the inversion process is extremely user-dependent. Using earthquake recordings enables direct and in situ measurement of wave propagation along a borehole, taking into account the complex geomorphology of the site as well as the variability related to earthquake characteristics.

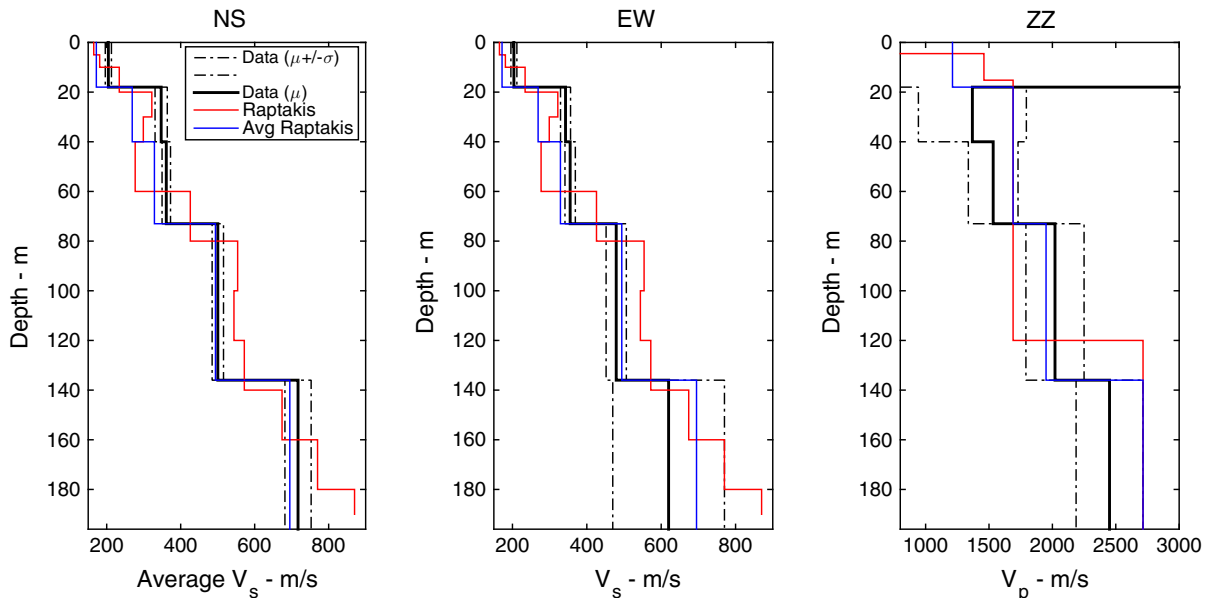


Figure 3

Shear (NS and EW) and compressive (ZZ) velocity profiles obtained by seismic interferometry by deconvolution using all the recordings. Soil profiles are compared with the RAPTAKIS *et al.* (2000) velocity profile based on geotechnical and geophysical surveys. The blue line is the interpreted Raptakis profile, considering the positions of the borehole sensors. For  $V_p$ , shear wave velocity in the upper layer is not well recognized due to the mixing of upward and downward waves, see Fig. 2

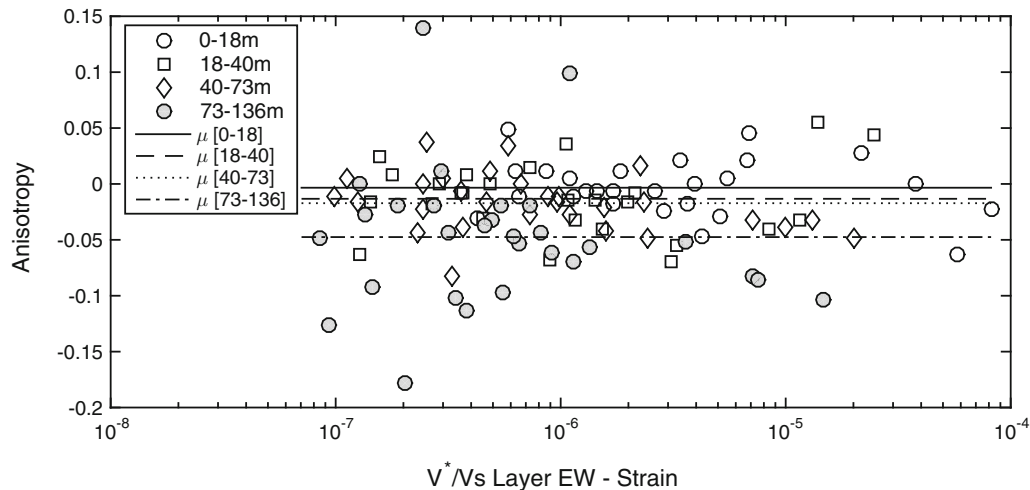


Figure 4

Horizontal anisotropy of shear wave velocity with respect to depth along the borehole. Anisotropy is computed as  $(V_{SEW} - V_{SNS})/V_{SEW}$  and represented with respect to the strain proxy in the EW direction

Velocity by deconvolution is therefore reliable and accurate enough to observe a slight variation related to the physical process of wave propagation. For example, slight differences are observed between horizontal components, suggesting slight horizontal anisotropy in terms of shear wave velocity. Anisotropy increases with depth (Fig. 4), with values less than 5 % between the EW and NS directions and stable with the level of strain computed along the borehole (see below for the definition of strain). Additional reasons could be invoked and explored to explain the difference of wave velocity in the two horizontal directions that may be at the origin of the dispersion of values observed in Fig. 4. However,  $V_s$  computed by deconvolution reflects the elastic property of the material and the tendency at each depth seems to reflect anisotropy. Moreover, COUTANT (1996) and, more recently, CHANDRA *et al.* (2015) also reported such anisotropy related to shear wave velocity at the Garner-Valley Californian vertical array, the latter authors using seismic interferometry by deconvolution. Anisotropy has never been reported by classical geophysical invasive or non-invasive methods. This anisotropy has a relatively slight effect on the prediction of seismic ground motion or seismic site effects but thanks to the efficiency and accuracy of seismic interferometry for shear wave velocity assessment, each earthquake can be considered as a

single, in situ, real-scale cyclic test and the nonlinear response of the site can be studied by observing the variation (however small) of shear wave velocity with respect to the loading.

#### 4. Shear Stress and Shear Strain Assessment

Based on the direct wave propagation approach, ZEGHAL *et al.* (1995) proposed an alternative way to estimate stress–strain relationships using a vertical accelerometric array. Basically, linear interpolation between horizontal acceleration recordings from two successive sensors provides a first-order estimate of shear stress. The same approach is considered for shear strain, considering the linear interpolation of the horizontal displacement divided by the distance between the sensors. Considering all the available sensors, a first order estimate of the shear stress–strain relationship can be computed for each earthquake and each position along the borehole. Based on a more comprehensive interpretation, RATHJE *et al.* (2004) defined equivalent shear stress as the spatial derivative of acceleration  $A^*$ , expressed as follows:

$$\tau = A^* \rho z \quad (6)$$

where  $\rho$  is the density of the soil, and  $A^*$  the linear interpolation of horizontal acceleration at depth  $z$ , i.e.

corresponding to the intermediate point between two successive sensors. Assuming a rather limited variation of density,  $A^*$  is a proxy of shear stress and is computed thus:

$$A^* = \left[ \frac{|a_i(t) - a_j(t)|}{2} \right]_{\max} \quad (7)$$

where  $a_i(t)$  and  $a_j(t)$  correspond to horizontal acceleration at two successive sensors  $i$  and  $j$ . In the same manner, shear strain can be expressed by the spatial derivative displacements ( $u$ ) as follows:

$$\gamma = \frac{du}{dz} \quad (8)$$

CHANDRA *et al.* (2015) tested different ways of computing the relative displacement based strain  $\gamma_1$ , depending on whether or not maximum displacement is considered to occur at the same time on the two sensors. For our study, we adopted the solution producing the least variation, according to CHANDRA *et al.* (2015), i.e.:

$$\gamma_1 = \left| \frac{u_i(t) - u_j(t)}{(z_i - z_j)} \right|_{\max} \quad (9)$$

with  $z_i - z_j$  the distance between two successive sensors.

From Eq. 8, a shear strain proxy  $\gamma_2$ , as proposed by HILL *et al.* (1993), can be computed, considering the time derivative solution of Eq. 8 as follows:

$$\gamma_2 = \frac{du}{dz} = \frac{du/dt}{dz/dt} = \frac{V^*}{Vs} \quad (10)$$

in which  $du/dt$  corresponds to the velocity of the particle motion  $V^*$  and  $dz/dt$  to the velocity of wave propagation  $Vs$ . As for acceleration  $A^*$ ,  $V^*$  is the linear interpolation of the horizontal velocity recordings ( $v(t)$ ) from two successive sensors, i.e.,

$$V^* = \left[ \frac{|v_i(t) - v_j(t)|}{2} \right]_{\max} \quad (11)$$

and  $Vs$  is the specific shear-wave velocity computed by seismic interferometry during each earthquake. Velocity and displacement are calculated by integrating and double integrating acceleration following the procedure proposed by BOORE (2005). This method implicitly transforms the signals to obtain the

same length, by applying zero padding before filtering and integration.

The shear stress–strain relationship ( $A^* - \gamma$ ) is thus obtained for each earthquake from  $\gamma_1$  to  $\gamma_2$ . Figure 5 compares  $\gamma_1$  and  $\gamma_2$  values for all earthquakes and at all depths along the TST borehole. A good fit is observed between both approaches in the two horizontal directions, with very slight differences. The linear model gives 93 % (>66 %) and 95.5 % (>95 %) of the residues computed using the model and experimental data between  $\pm\sigma$  and  $\pm 2\sigma$ , respectively, allowing us to conclude on the normal distribution of the residues and the efficiency of the  $\gamma_2 = V^*/Vs$  strain proxy. In the rest of this manuscript, the strain parameter is related to the shear strain proxy  $\gamma_2$  (Eq. 10).

In Fig. 5, strain values range from  $10^{-7}$  to  $10^{-4}$ , i.e. earthquake data recorded at the TST site produce relatively small amplitude of strain. Usually, the largest strain occurs in the uppermost layer, where the nonlinear response may be more pronounced. In fact, the nonlinear response is generally expected to be found in the uppermost sedimentary layer, which is why nonlinear analyses based on laboratory tests are focused on such materials. However, GÉLIS and BONILLA (2012b) obtained numerically nonlinear effects in deep sediments, related to the frequency dependence of nonlinear effects, and CHANDRA *et al.* (2015) observed nonlinear response even in the deepest layers of Californian boreholes. At the TST site, we observed strain values in the deepest layers large enough to generate nonlinearities. VUCETIC (1994) actually distinguished two different shear strain thresholds related to soil nonlinearity: below the linear cyclic  $\gamma_{il}$  threshold, soil has a linear response; above the volumetric  $\gamma_{iv}$  threshold, soil shows hysteretic behavior with permanent deformation; and for  $\gamma_{il} < \gamma < \gamma_{iv}$ , soil has a nonlinear elastic response without (or with only negligible) permanent deformation. Standard strain values for  $\gamma_{il}$  and  $\gamma_{iv}$  are relatively scattered but an order of magnitude for  $\gamma_{iv}$  of around  $10^{-4}$  (HARDIN and BLACK 1968; DRNEVICH and RICHART 1970; DOBRY and LADD 1980; YOUNG 1972; VUCETIC 1994) and less than  $10^{-6}$  for  $\gamma_{il}$  (Vucetic 1994; JOHNSON and JIA 2005) lead us to expect to observe nonlinear response at the TST site.



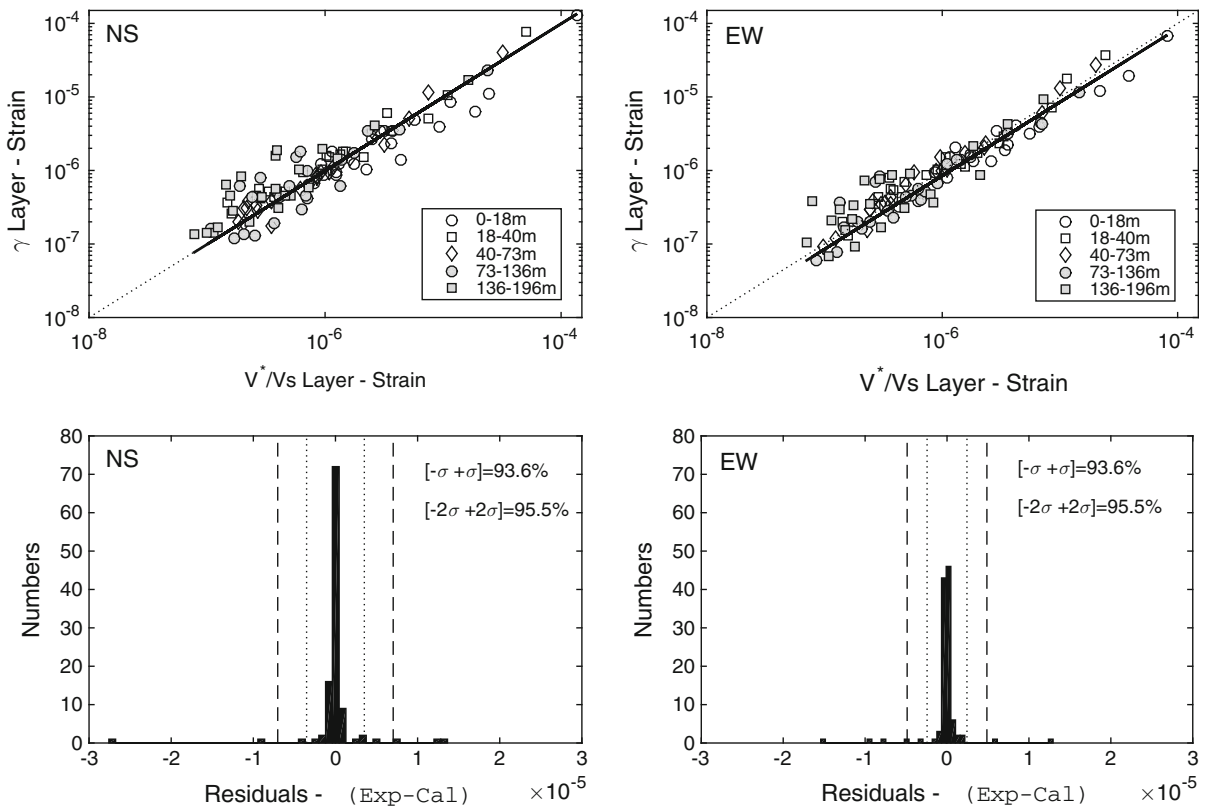


Figure 5

Comparing strain along the TST borehole computed as  $\gamma$ , the relative time displacement between each sensor divided by distance, and as the strain proxy,  $V^*/V_s$ ,  $V^*$  corresponding to the average velocity between the sensors (see CHANDRA *et al.* 2015 for the definition)

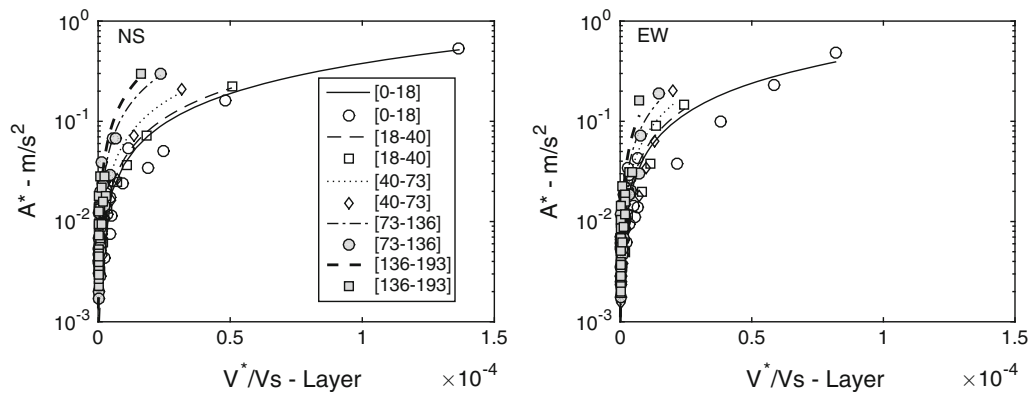


Figure 6

Acceleration  $A^*$  vs strain computed as a  $V^*/V_s$  proxy at different depths along the TST borehole in the NS (*left*) and EW (*right*) directions. The interpolation curves correspond to the fit of the data, based on the hyperbolic nonlinear model (see CHANDRA *et al.* 2015 for explanation)

The nonlinear response can also be confirmed in Fig. 6, displaying the stress–strain relationship for all events in the horizontal direction and at every depth. Although the data at GL-196 show significant variability in the east–west direction, they are included because the results are also relevant in terms of nonlinear response at greater depths. For each depth, a hyperbolic model is fitted to the data, based on the conventional model of the nonlinear stress–strain relationships given by SEED *et al.* (1984) and ISHIHARA (1996), modified by CHANDRA *et al.* (2015):

$$A^* = \frac{a\gamma_2}{1 + \gamma_2 \frac{a}{b}} \quad (12)$$

with  $a$  and  $b$  being two parameters proportional to the shear modulus and the reference strain corresponding to the ratio between maximum shear stress and maximum shear modulus. In a theoretical model, the slope of the hyperbolic model changes after the yield strain, which reproduces basically the nonlinearity effect. In Fig. 6, the hyperbolic models show a larger nonlinear response in the uppermost layers than in the deeper layers. Nonlinear response is quasi similar in the two first layers (GL-0-GL-18 and GL-18-GL-40). In these cases, yield strains appear at small strain values around  $5 \cdot 10^{-6}$ , i.e. equivalent to the conventional values of the linear cyclic  $\gamma_H$  threshold. Nonlinear responses are also observed in the deepest layers, but the same acceleration produces smaller values of strain than in the uppermost layers. The nonlinear response is also confirmed by Fig. 7 which compares the in situ and laboratory experiment  $G/G_{\max}$ - $\gamma$  curve generally used to represent the nonlinear response of soil. Laboratory tests results provided by RAPTAKIS *et al.* (2000) were obtained from samples located in the shallow layers. Because strain, shear velocity and stress values from accelerometric data are obtained between sensors, we compared the shear degradation models compatible with the TST sediment layers, without distinction of each layer considered by RAPTAKIS *et al.* (2000). In our case, we assume constant density and  $G/G_{\max}$  is considered as  $V_s/V_{s\max}$  with  $V_{s\max}$ , the mean value of shear wave velocity, computed by seismic interferometry and for strain values below  $10^{-6}$ . As in Fig. 6, we observe

the largest strain values in the uppermost layers, nonlinear degradation of shear velocity at about  $5 \cdot 10^{-6}$ , i.e. equivalent to the  $\gamma_H$  threshold and also slight nonlinearity even in the deepest layers (as mentioned previously, the GL-136-GL-196 data are too scattered to be able draw conclusions on nonlinearity). By computing the mean value of  $V_s$  for different strain ranges, the variation of  $V_s$  between  $10^{-6}$  and  $10^{-5}$  of strain is 0.1 % and between  $10^{-6}$  and  $10^{-4}$  is about 4 %. As shown in Figs. 6 and 7, the data are not strong enough to enable definitive conclusions to be made on the nonlinear response at depth, however, the equivalent in situ stress–strain ( $A^* - \gamma$ ) relationship based on the strain proxy  $V^*/V_s$  does provide comprehensible information on the nonlinear response of the site. These two parameters, i.e.  $A^*$  and  $V^*/V_s$ , are equivalent to shear stress and strain and in situ earthquake recordings provide reliable information that can be used to account for the effect of nonlinear site response in site-specific ground motion predictions.

##### 5. Analysis of Nonlinear Response for the Site-Specific Prediction of Ground Motion

$V_s30$  is a convenient parameter used in earthquake engineering and engineering seismology for site classification. For site-specific predictions,  $V_s30$  is obtained by computing the average time travel time of the shear wave between GL-0 and GL-30 and invasive or non-invasive geophysical methods are employed to obtain shear wave velocity profiles.  $V_s30$  is introduced as a site parameter in ground motion prediction equations in order to reduce or at least identify uncertainties in the predicted ground motion. CHOI and STEWART (2005) showed that nonlinearity is dependent on  $V_s30$  and the degree of nonlinearity is higher for soft soil classified according to  $V_s30$  (<180 m/s). Keeping in mind the primary objective of this paper, i.e. predicting the nonlinear seismic response of sites using a simple proxy, a  $V_s30$ -based strain proxy was tested, as proposed by IDRIS (2011). In this case, we adopted a pragmatic approach, i.e. to estimate site nonlinearity using only

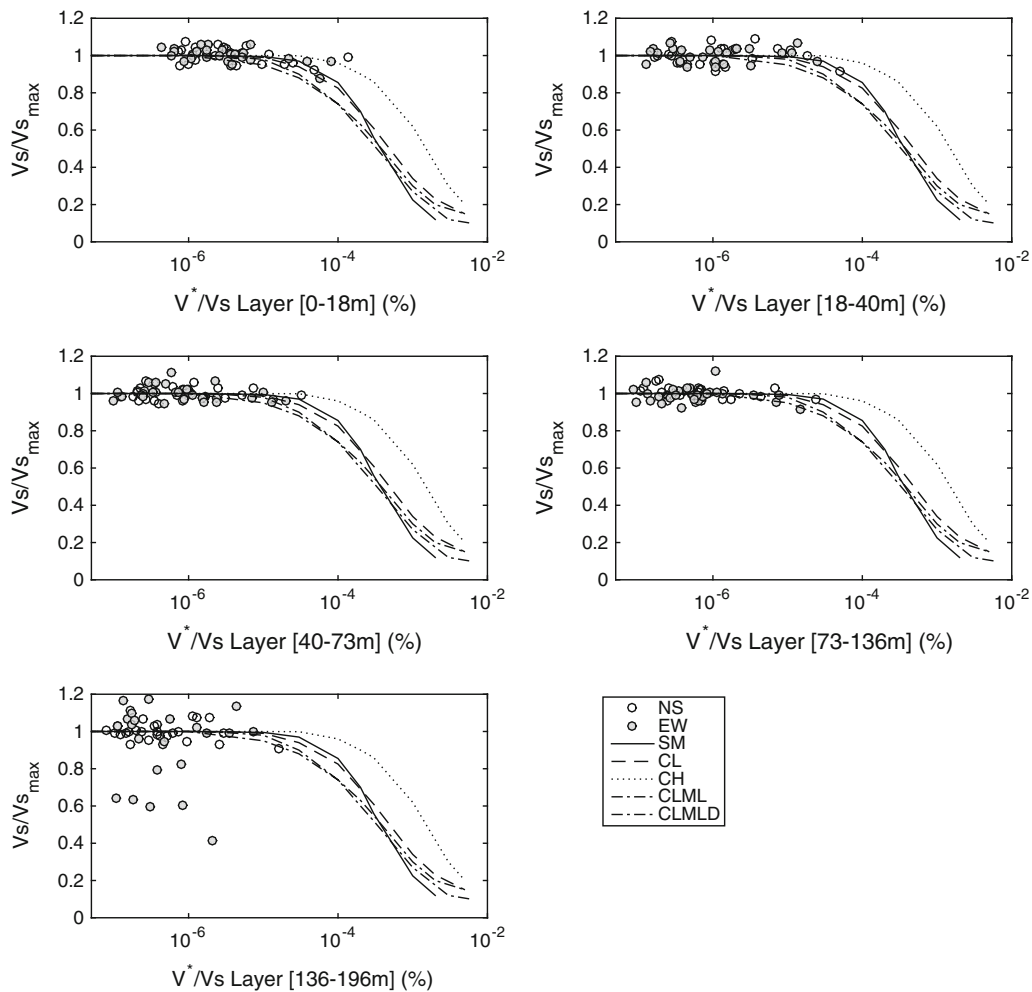


Figure 7

$V_s/V_{s_{max}}$  vs strain proxy at different depths along the TST borehole in the NS (*open circles*) and EW (*filled circles*) compared with the theoretical  $G - \gamma$  curves considered for each TST soil layer by RAPTAKIS *et al.* (2005).  $V_{s_{max}}$  is considered as the average value of velocity corresponding to  $V^*/V_s$  below  $10^{-6}$

GL-0 earthquake recordings, without using the vertical accelerometer array. Consequently, the stress-strain relationship is considered as  $PGA$  vs  $PGV/V_{s30}$ , with  $PGA$  and  $PGV$  being peak ground acceleration (equivalent shear stress) and peak ground velocity.

RAPTAKIS *et al.* (2000) computed  $V_{s30}$  equal to 200 m/s at the TST site. Herein, the stress-strain relationships considering  $PGA/PGV/V_{s30}$  or  $A^*/V^*/V_s$  measured in the GL0-GL40 m layer are shown in Fig. 8, differentiated by the NS and EW directions.

$PGV/V_{s30}$  slightly overestimates the strain value given by  $V^*/V_s$ . However, whatever the strain proxy, nonlinearity exhibits non-negligible curvature and yield strain is ranging from about  $5 \cdot 10^{-6}$  and  $5 \cdot 10^{-5}$ . It is difficult to accurately and objectively assess the yield strain for sparse and discrete data. A bilinear model is approximated to the data by adjusting a piecewise linear model to the strain values lower and larger than  $10^{-5}$  (Fig. 8). The yield strain is  $2 \cdot 10^{-5}$  in this case but this remains an approximate value that must be confirmed with additional in situ

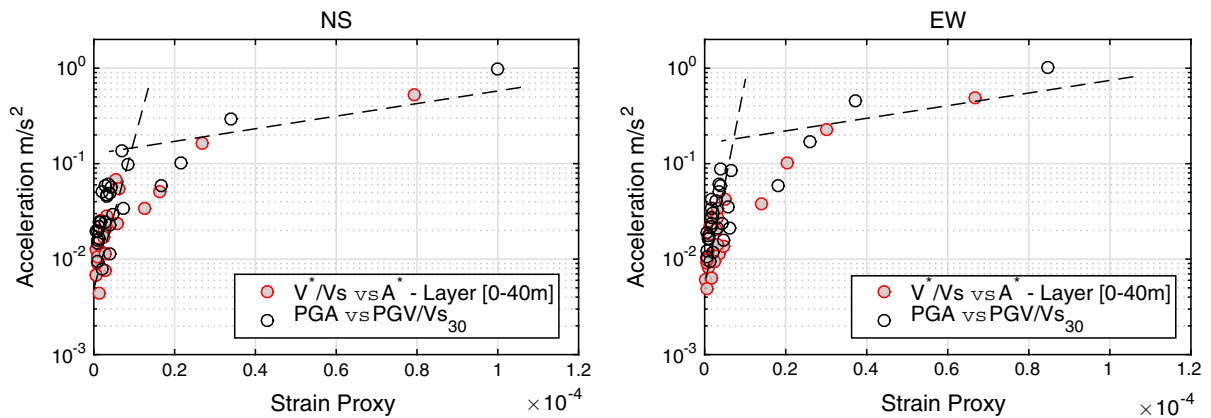


Figure 8

Acceleration recorded at the near surface vs the strain proxy considering  $PGA/PGV/Vs_{30}$  parameters or  $A^*/V^*/Vs$  in the GL0-GL40 m layer in the NS (left) and EW (right) directions. Dashed lines are the approximation of the bi-linear model done by a piecewise linear fit applied to the data smaller and larger than  $10^{-5}$  of strain, respectively

stronger data. At low strain, two branches are distinguished along which the data are distributed, with different strain values for equivalent acceleration values. This difference may be the result of the proxy considered. The proxy does not take into account all the physical processes that make up the phenomenon, but it does provide an indirect representation of certain behavior patterns. For example, YU *et al.* (1993), DER NI *et al.* (2000) and GÉLIS and BONILLA (2012a, b) reported the frequency dependence of the seismic nonlinearity of sedimentary sites and/or the magnitude or distance effect not accounted for in the  $PGV/Vs_{30}$  ratio.

In order to better constrain the significance of the strain proxy, Fig. 9 shows the results of several tests that were carried out to take into account (Fig. 9a) the year of the earthquake, based on the suspicion of possible long-term degradation of the TST site, (Fig. 9b) the azimuth of the earthquake because of the 3D shape of the Volvi basin, and (Fig. 9c) the distance of the earthquake. No dependency of the site's nonlinear response was observed with year and azimuth, regardless of the horizontal component. Strain values were not distributed according to these two parameters and the same two branches at low strain values were observed on the stress-strain relationship. This observation is the same considering

$PGV/Vs_{30}$  or  $V^*/Vs$  (0–40 m) as the strain proxy. On the contrary, Fig. 9c shows clear distance dependency of the nonlinear behavior of the site. For short distance earthquakes, seismic ground accelerations produce less nonlinearity in the uppermost layer than for long distance events, and the two branches of the stress-strain curve at low strain values are entirely controlled and distributed according to the distance of the earthquakes. This observation is the same in both horizontal directions and reflects the effect of the nature of the seismic wavefield generated by the earthquake according to distance. This can be related to the proportion of body and surface waves recorded, particularly in a shallow sedimentary basin like the Volvi basin, where the proportion of surface waves is high. On the other hand, the geometrical attenuation of the propagation modifies the frequency content of the wavefield, seismic ground motion at high frequency being stronger in the near-field domain than in the far-field.

Since frequency dependence was suspected, we investigated the relative influence of the period of the response spectra considered as stress. Accelerometric response spectra ( $S_a$ ) were computed for 5 % critical damping and mean response spectra were computed for four ranges of period  $T$ , i.e. (0.1–0.3), (0.3–1.0), (1.0–3.0) and (3.0–5.0) s. Figure 10 shows the stress–

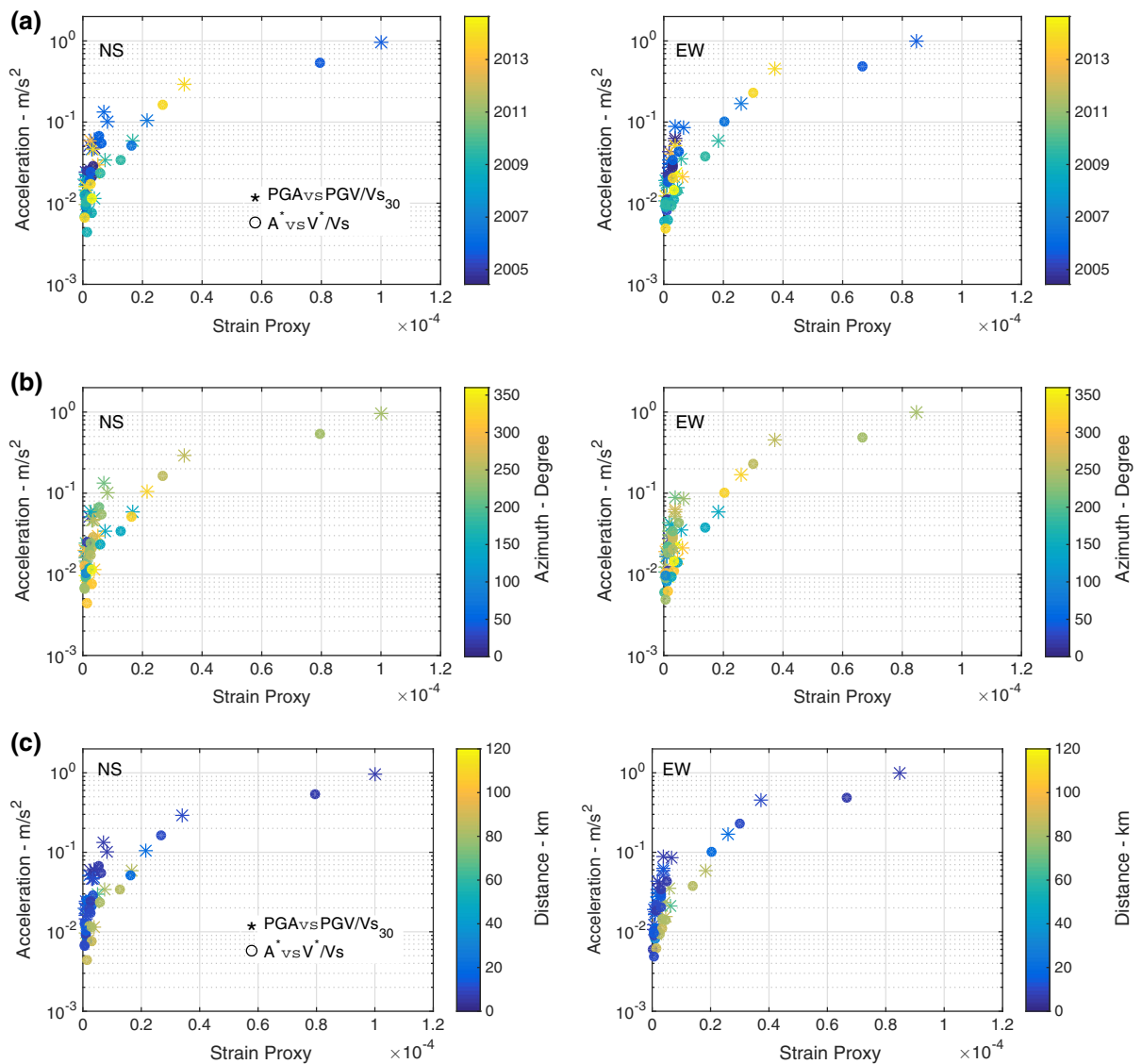
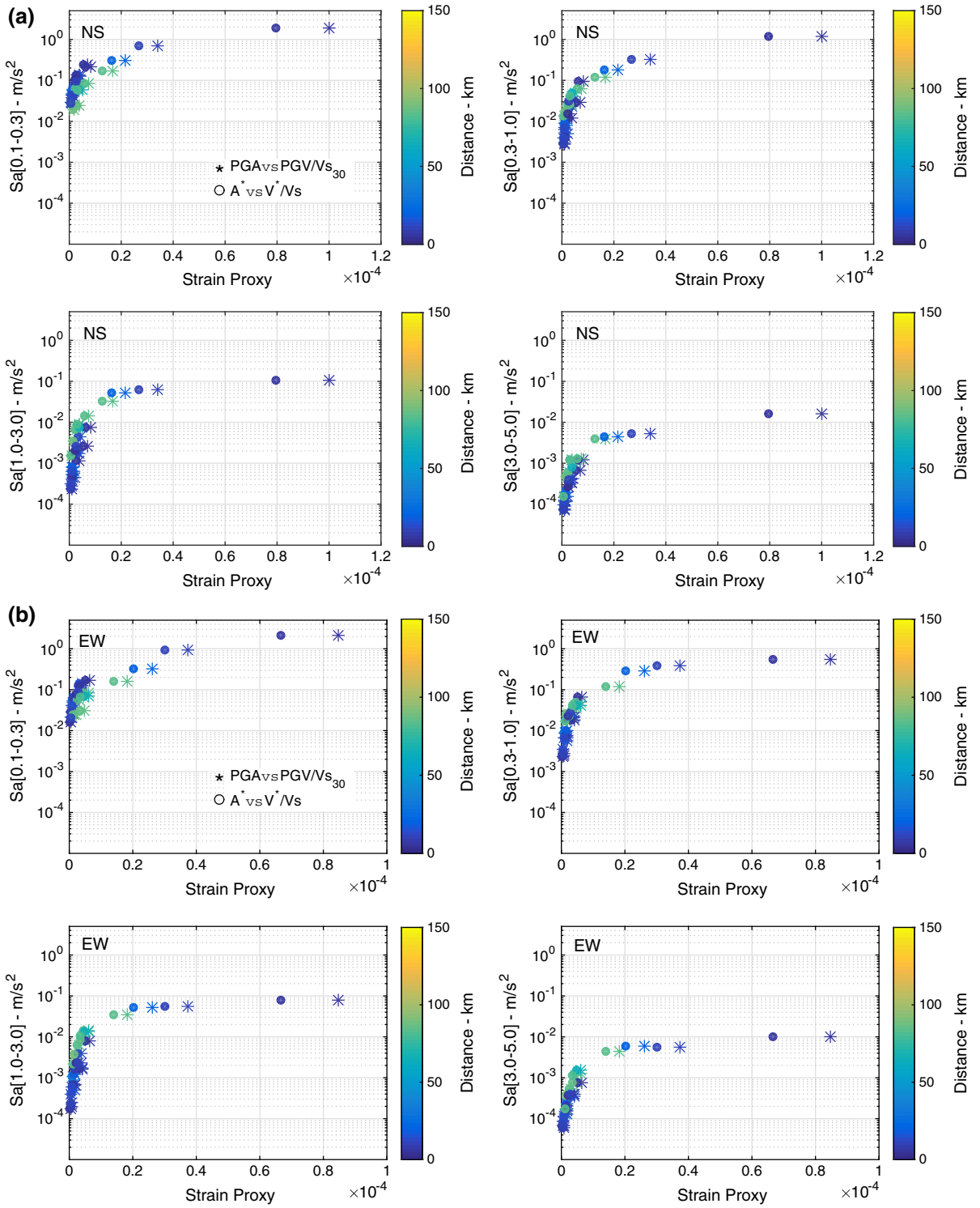


Figure 9  
Idem Fig. 8 considering year (a), azimuth (b) and distance (c) of the earthquakes

strain relationships considering  $Sa(T)$  as stress, and  $PGV/Vs_{30}$  and  $V^*/Vs$  (0–40 m) as strain. As in Figs. 8 and 9, the yield strain is ranging from about  $5 \cdot 10^{-6}$  and  $5 \cdot 10^{-5}$  in the EW and NS directions. The bilinear approximation gives yield strain at  $2 \cdot 10^{-5}$ ,  $2.5 \cdot 10^{-5}$ ,  $1.8 \cdot 10^{-5}$  and  $2.0 \cdot 10^{-5}$  for (0.1–0.3), (0.3–1.0), (1.0–3.0) and (3.0–5.0) s, respectively. For a given stress value, the variability of strain is smaller and the stress–strain curve is without uncertainties. This is particularly true for periods above 0.3 s: since

PGA characterizes the high-frequency ground motion, this observation confirms that PGA is a less efficient parameter for characterizing seismic ground motion and predicting the nonlinear response of soil. It is important to note that the nonlinear response is the same in the NS (Fig. 10a) and EW (Fig. 10b) directions, but also for different distances, whatever the period range. This confirms the relevance of the  $Sa-PGV/Vs_{30}$  relationship for predicting the nonlinear response of the site.



◀Figure 10

Acceleration response spectra at GL-0 m, averaged between four period ranges [(0.1–0.3 s); (0.3–1.0 s); (1.0–3.0 s); (3.0–5.0 s)] vs the strain proxy at the near surface considering  $PGA/PGV/Vs30$  parameters or  $A^*/V^*/Vs$  in the GL0-GL40 m layer in the NS **a** and EW **b** directions and according to earthquake distance

## 6. Conclusions

We have presented the analysis of the Volvi TST site based on situ accelerometric data to explore its nonlinear behavior. The response was analyzed by in situ stress–strain relationships during earthquakes, considering each earthquake as an in situ cyclic test. Strain was computed by different methods, based on the relative displacement between two successive sensors along the borehole or a strain proxy based on particle velocity and shear wave velocity. First, the shear wave velocity between the sensors was computed by seismic interferometry, a method that provides an efficient tool to obtain a velocity profile compared with invasive and non-invasive geophysical methods reported by RAPTAKIS *et al.* (2000). Using this method, we were able to compute degradation of the shear-wave velocity and to analyze the nonlinear response of the site. We are aware that the accuracy of the  $V_s$  values calculated by deconvolution is not addressed comprehensively in the manuscript. Previous studies have shown that it is possible to detect accurately small variations of  $V_s$ , related to atmospheric conditions (NAKATA and SNIEDER 2012) or to the anisotropy of  $V_s$  in the horizontal directions (CHANDRA *et al.* 2015). At constant strain, we observed slight changes in  $V_s$  values, as in Fig. 4. At this stage it is difficult to assess the accuracy of  $V_s$ , without more data available: other parameters can have an important impact such as the magnitude, distance or azimuth of seismic events. This question on the accuracy of the estimate of seismic interferometry by  $V_s$  will be discussed in further studies through numerical simulations.

Applied to the TST Volvi site, the strain proxy based on the velocity ratio ( $V^*/V_s$ ) is comparable to direct displacement-based strain. Assuming constant density, nonlinearities were observed on the  $G/G_{\max}$  (or  $V_s/V_{s_{\max}}$ ) –  $\gamma$  curves, coherent with the theoretical curves assumed for the sedimentary layers at the Volvi TST site. Note that nonlinearity was also observed at depth, even though there are not enough data to allow

us to draw definitive conclusions. However, nonlinearities were also reported on stress–strain curves, considering acceleration as the stress value. We checked that accelerometric response spectra and  $PGV/Vs30$  appear to be efficient stress–strain proxies that reproduce the theoretical nonlinear response of sites as well as possible. Nonlinearity appears at a strain of  $5 \cdot 10^{-6}$ – $5 \cdot 10^{-5}$ , i.e. a threshold equivalent to the values also reported by VUCETIC (1994) and JOHNSON and JIA (2005). Note that the  $S_a$  values for longer periods are more stable as stress parameters than  $PGA$  and independent of the azimuth or the distance of earthquakes. However, accelerometric data at Volvi are weak and stronger seismic ground motions are needed in order to exhaustively confirm the efficiency of the proposed proxy for larger deformation.

However,  $Vs30$  uncertainties are a critical issue for prediction of ground motion. This study confirms the good prediction of the nonlinear response of sites using the  $PGV/Vs30$  strain proxy derived from in situ data. This proxy might ultimately be integrated into ground motion predictions, including nonlinearity rather than just  $Vs30$ , and site-specific analysis including nonlinear response could be performed directly using in situ accelerometric data and used to reduce the epistemic uncertainties related to site conditions in ground motion prediction equations. This is an argument for continuing to maintain vertical array and develop specific array close to large infrastructure so we can observe, insitu, the full degradation curve as larger motions (stresses and strains) are observed in time.

## Acknowledgments

This study was sponsored by the Urban Seismology project at the Institute of Earth Science ISTerre of the University of Grenoble-Alpes. We thanks Zafeiria Roumelioti from Aristotle University of Thessaloniki to have prepared the data.

## REFERENCES

- ABRAHAMSON, N. A., SILVA, W. J., and KAMAI, R. (2014), *Summary of the ASK14 Ground Motion Relation for Active Crustal Regions*, *Earthquake Spectra*, 30(3), 1025–1055.

- ASSIMAKI, D., LI, W., STEIDL, J.H., and TSUDA, K. (2008), *Site Amplification and Attenuation via Downhole Array Seismogram Inversion: A comparative Study of the 2003 Miyagi - Oki Aftershock Sequence*, Bulletin of the Seismological Society of America, 98(1), 301-330.
- BERESNEV, I.A., ATKINSON, G.M., JOHNSON, P.A., and FIELD, E.H. *Stochastic Finite-Fault Modeling of Ground Motions from the 1994 Northridge, California, Earthquake. II. Widespread Nonlinear Response at Soil Sites*. Bulletin of the Seismological Society of America, 88(6): 1402-1410 (1998).
- BONILLA, L.F., ARCHULETA, R.J., and LAVALLÉE, D. (2005), *Hysteretic and Dilatant Behavior of Cohesionless Soils and Their Effects on Nonlinear site Response: Field Data Observations and Modeling*, Bulletin of the Seismological Society of America, 95(6), 2373-2395.
- BONILLA, L.F., TSUDA, K., PULIDO, N., REGNIER, J., and LAURENDEAU, A. (2011), *Nonlinear Site Response Evidence of K-Net and KiK-net Records from the 2011 off the Pacific coast of Tohoku Earthquake*, Earth Planets Space, 63, 785-789.
- BOORE, D. *On Pads and Filters: Processing Strong-Motion Data*. Bulletin of the Seismological Society of America, 95(2): 745-750 (2005).
- BOORE, D. M., STEWART, J. P., SEYHAN, E., and ATKINSON, G. M. (2014), *NGA-West2 Equations for Predicting PGA, PGV, and 5% Damped PSA for Shallow Crustal Earthquakes*, Earthquake Spectra, 30(3), 1057-1085.
- CHANDRA, J., GUÉGUEN, P., STEIDL, J. H., and BONILLA, L. F. (2015), *In-situ Assessment of the G- $\gamma$  Curve for Characterizing the Nonlinear Response of Soil: Application to the Garner Valley Downhole Array(GVDA) and the Wildlife Liquefaction Array (WLA)*, Bulletin of Seismological Society of America, 105(2A), 993-1010.
- CHOI, Y., and STEWART, J.P. (2005), *Nonlinear Site Amplification as Function of 30 m Shear Wave Velocity*, Earthquake Spectra, 21(1), 1-30.
- CLAYTON, R.W., and WIGGINS, R.A. (1976), *Source shape estimation and deconvolution of teleseismic bodywaves*, The Geophysical Journal of the Royal Astronomy Society, 47, 151-177.
- COUTANT, O. (1996), *Observation of Shallow Anisotropy on Local Earthquake Records at the Garner Valley, Southern California, Downhole Array*, Bulletin of the Seismological Society of America, 86(2), 477-488.
- DE MARTIN, F., H. KAWASE, and F. BONILLA (2012). *Inversion of equivalent linear soil parameters during the 2011 Tohoku earthquake, Japan, JST/ANR Joint Research ONAMAZU Project-International Symposium on Engineering Lessons Learned from the Giant Earthquake*, Kenchiku-kaikan, Tokyo, Japan, 1-4 March.
- DER NI, S., ANDERSON, J.G., ZENG, Y., and SIDDHARTHAN, R.V. (2000), *Expected Signature of Nonlinearity on Regression for Strong Ground-Motion Parameters*, Bulletin of the Seismological Society of America, 90, S53-S64.
- DERODE, A., LAROSE, E., TANTER, M., DE ROSNY, J., TOURIN, A., CAMPILLO, M., and FINK, M. (2003), *Recovering the Green's Function from Field-Field Correlations in an Open Scattering Medium*, The Journal of the Acoustical Society of America, 113(6), 2973-2976.
- DOBRY, R., and LADD, R. (1980), *Discussion of 'Soil liquefaction and cyclic mobility evaluation for level ground during earthquakes,' by H.B. Seed and 'Liquefaction potential: science versus practice,' by R. B. Peck*, Journal of the Geotechnical Engineering Division, 106(6), 720-724.
- DRNEVICH, V. P., and RICHART, F. E. (1970), *Dynamic Prestraining of Dry Sand*, Journal of Soil Mechanics and Foundations Division, 96(2), 453-469.
- GÉLIS, C., and BONILLA, F. (2012), *2D P-SV Numerical Study of Soil-Source Interaction in a Nonlinear Basin*, Geophysical Journal International, 191(3), 1374-1390.
- HARDIN, B. O., and BLACK, W. L. (1968), *Vibration Modulus of Normally Consolidated Clay*, Journal of Soil Mechanics and Foundations Division, 94(2), 353-369.
- HILL, D. P., REASENBERG, P. A., MICHAEL, A., ARABAZ, W.J., BEROZA, G., BRUMBAUGH, D., BRUNE, J. N., CASTRO, R., DAVIS, S., DEPOLO, D., ELLSWORTH, W. L., GOMBERG, J., HARMSSEN, S., HOUSE, L., JACKSON, S. M., JOHNSTON, M. J. S., JONES, L., KELLER, R., MALONE, S., MUNGUIA, L., NAVA, S., PECHMANN, J. C., SANFORD, A., SIMPSON, R. W., SMITH, R. B., STARKS, M., STICKNEY, M., VIDAL, A., WALTER, S., WONG, V., and ZOLLWEG, J. (1993), *Seismicity Remotely Triggered by the Magnitude 7.3 Landers, California, Earthquake*, Science, 260, 1617-1623.
- DIMITRIU, P., THEODULIDIS, N., HATZIDIMITRIU, P., and ANASTASIADIS, A. (2001), *Sediment Nonlinearity and Attenuation of Seismic Waves; A Study of Accelerograms from Mefkas, Western Greece*, Soil Dynamics and Earthquake Engineering, 21, 63-73.
- FIELD, E.H., JOHNSON, P.A., BERESNEV, I., and ZENG, Y. (1997), *Nonlinear ground-motion amplification by sediments during the 1994 Northridge earthquake*, Nature, 390, 599-602.
- FRANKEL, D.A., (1999), *How Does the Ground Shake ?*, Science, 283(5410), 2032-2033
- FRANKEL, A.D., CARVER, D.L., and WILLIAMS, R.A. (2002), *Nonlinear and Linear Site Response and Basin Effects in Seattle for the M 6.8 Nisqually, Washington, Earthquake*, Bulletin of the Seismological Society of America, 92(6), 2090-2109.
- GÉLIS, C., and BONILLA, F. (2012), *2D P-SV Numerical Study of Soil-Source Interaction in a Nonlinear Basin*, Geophysical Journal International, 191(3), 1374-1390.
- IDRISS, I.M. (2011), *Use of  $V_{s30}$  to represent Local site Condition, 4th IASPEI/IAEE International Symposium. Effects of Source Geology on Seismic Motion*. August 23-26th, 2011. University of Santa Barbara California.
- ISHIHARA, K. *Soil Behaviour in Earthquake Geotechnics* (Oxford Engineering Science Series. Oxford University Press, 1996).
- JONGMANS, D., PITILAKIS, K., DEMANET, D., RAPPAKIS, D., RIEPL, J., HORRENT, C., TSOKAS, G., LONTZETIDIS, K., and BARD, P.-Y. (1998), *EURO-SEISTEST: Determination of the Geological Structure of the Volvi Graben and Validation of the Basin Response*, Bull. Seismol. Soc. Am. 88, 473-487.
- JOHNSON, P.A., and JIA, X. P. (2005), *Nonlinear Dynamics, Granular Media and Dynamic Earthquake Triggering*, Nature, 437, 871-874.
- KIM, B., HASHASH, Y., RATHJE, E. M., STEWART, J. P., NI, S., SOMERVILLE, P. G., KOTTKE, A. R., SILVA, W. J., and CAMPBELL, K.W. (2015), *Subsurface shear-wave velocity characterization using P-wave seismograms in Central and Eastern North America*, Earthquake Spectra In-Press, doi:10.1193/123013EQS299M
- LOBKIS, O. I., and WEAVER, R. L. (2001), *On the Emergence of the Green's function in the Correlations of a Diffuse Field*, The Journal of the Acoustical Society of America, 110(6), 3011-3017.
- MANAKOÛ, M.V., RAPPAKIS, D.G., CHÁVEZ-GARCÍA, F.J., APOSTOLIDIS, P.I., and PITILAKIS, K.D. (2010), *3D Soil Structure of the*



- Mygdonian Basin for Site Response Analysis*, Soil Dyn. Earthq. Eng., 30(11), 1198–1211.
- MEHTA, K., SNIEDER, R., and GRAIZER, V. (2007), Downhole Receiver Function: a Case Study. Bulletin of the Seismological Society of America, 97(5), 1396–1403.
- NAKATA, N., and SNIEDER, R. (2011), *Near Surface Weakening in Japan after the 2011 Tohoku-Oki Earthquake*, Geophysical Research Letters, 38: L17302.
- NAKATA, N., and SNIEDER, R. (2012), *Estimating near-surface wave velocities in Japan by applying seismic interferometry to KiK-net data*. Journal of Geophysical Research, 117: B01308.
- PAVLENKO, O., and IRIKURA, K. (2002), *Changes in Shear Moduli of Liquefied and Nonliquefied Soils during the 1995 Kobe Earthquake and its Aftershocks at Three Vertical-Array Sites*, Bulletin of the Seismological Society of America, 92(5), 1952–1969.
- PAVLENKO, O., and IRIKURA, K. (2003), *Estimation of Nonlinear Time-Dependent Soil Behavior in Strong Ground Motion Based on Vertical Array Data*, Pure and Applied Geophysics, 160, 2365–2379.
- PECH, A., SÁNCHEZ-SESMA, F. J., SNIEDER, R., IGNICIO-CABALLERO, F., RODRÍGUEZ-CASTELLANOS, A., and ORTÍZ-ALEMÁN, J.C. (2012), *Estimate of shear wave velocity, and its time-lapse change, from seismic data recorded at the SMNH01 station of KiK-net using seismic interferometry*, Soil Dynamics and Earthquake Engineering, 39:128–137.
- PITILAKIS, K., ROUMELIOTI, Z., RAPTAKIS, D., MANAKOU, M., LIAKAKIS, K., ANASTASIADIS, A., and PITILAKIS, D. (2013), *The EUROSEISTEST Strong Ground Motion Database and Web Portal*, Seismol. Res. Lett., 84(5), 796–804.
- RAPTAKIS, D., CHÁVEZ-GARCÍA, F.J., MAKRA, K., and PITILAKIS, K. (2000), *Site Effect at Euroseistest—I. Determination of the Valley Structure and Confrontation of Observations with 1D Analysis*, Soil Dyn. Earthq. Eng., 19(1), 1–22.
- RAPTAKIS, D.G., MANAKOU, M.V., CHÁVEZGARCÍA, F.J., MAKRA, K.A., and PITILAKIS, K.D. (2005), *3D Configuration of Mygdonian Basin and Preliminary Estimate of its Seismic Response*, Soil Dyn. Earthq. Eng., 25, 871–887.
- RAPTAKIS, D., and MAKRA, K. (2015), *Multiple Estimates of Soil Structure at a Vertical Strong Motion Array: Understanding Uncertainties from Different Shear Wave Velocity Profiles*, Engineering Geology, 192, 1–18.
- RATHJE, E. M., CHANG, W. J., STOKOE, K. H., and COX, B. R. (2004), *Evaluation of Ground Strain from In Situ Dynamic Response*, Proceeding of the 13th World Conference on Earthquake Engineering, Vancouver, B.C., Canada, August 1-6, Paper No. 3099.
- ROUMELIOTI, Z., and BERESNEV I. A. (2003), *Stochastic Finite-Fault Modeling of Ground Motions from the 1999 Chi-Chi, Taiwan, Earthquake: Application to Rock and Soil Sites with Implications for Nonlinear Site Response*. Bulletin of the Seismological Society of America, 93(4): 1691–1702.
- RUBINSTEIN, J.L., and BEROZA, G.C. (2004), *Evidence for Wide-spread Nonlinear Strong Ground Motion in the Mw 6.9 Loma Prieta Earthquake*, Bulletin of the Seismological Society of America, 94(5), 1595–1608.
- RUBINSTEIN, J.L., and BEROZA, G.C. (2005), *Depth Constraints on Nonlinear Strong Ground Motion from the 2004 Parkfield Earthquake*, Geophysical Research Letters, 32, L14313.
- SAWAZAKI, K., SATO, H., NAKAHARA, H., and NISHIMURA, T. (2009), *Time-Lapse Changes of Seismic Velocity in The Shallow Ground caused by Strong ground Motion Shock of the 2000 Western-Totoli Earthquake, Japan, as revealed from Coda Deconvolution Analysis*, Bulletin of the Seismological Society of America, 99(1), 352–366.
- SCHUSTER, G. T., YU, J., SHENG, J., and RICKETT, J. (2004), *Interferometric/daylight Seismic Imaging*. Geophysical Journal International, 157(2), 838–852.
- SEED, H.B., WONG, R.T., IDRIS, I.M., TOKIMATSU, T. (1984), *Moduli and Damping Factors for Dynamic Analyses of Cohesionless Soils*, Earthquake Engineering Research Center. Report No. UCB/EERC-84/14.
- SHAPIRO, N. M., CAMPILLO, M., STEHLY, L., and RITZWOLLER, M. H. (2005), *High-Resolution Surface-Wave Tomography from Ambient Seismic Noise*, Science, 307(5715), 1615–1618.
- SLEEP, N.H. (2010), *Nonlinear Behavior of Strong Surface Waves Trapped in Sedimentary Basins*, Bulletin of the Seismological Society of America, 100(2), 826–832.
- SNIEDER, R. (2004), *Extracting the Green's Function from the Correlation of Coda Waves: A Derivation Based on Stationary Phase*, Physical Review E, 69(4), 046610.
- SNIEDER, R., and ŞAFAK, E. (2006), *Extracting the Building Response Using Seismic Interferometry: Theory and Application to the Millikan Library in Pasadena, California*. Bulletin of the Seismological Society of America, 96(2), 586–598.
- SNIEDER, R., WAPENAAR, K., and LARNER, K. (2006), *Spurious Multiples in Seismic Interferometry of Primaries*, Geophysics, 71(4), S1111–S1124.
- VUCETIC, M. (1994), *Cyclic Threshold Shear Strains in Soils*, Journal of Geotechnical Engineering, 120, 2208–2228.
- WAPENAAR, K. (2004), *Retrieving the Elastodynamic Green's Function of an Arbitrary Inhomogeneous Medium by Cross Correlation*, Physical review letters, 93(25), 254301.
- WAPENAAR, K., DRAGANOV, D., SNIEDER, R., CAMPMAN, X., and VERDEL, A. *Tutorial on seismic interferometry: Part 1 – Basic principles and applications*. Geophysics, 75(5): 75A195–75A209 (2010).
- WU, C., PENG, Z., and ASSIMAKI, D. (2009), *Temporal Changes in Site Response Associated with the Strong Ground Motion of the 2004 Mw 6.6 Mid-Niigata Earthquake Sequences in Japan*, Bulletin of the Seismological Society of America, 99(6), 3487–3495.
- YOUND, T. L. (1972), *Compaction of Sands by Repeated Shear Straining*, Journal of Soil Mechanics and Foundation Engineering Division, 98(7), 709–725.
- YU, G., ANDERSON, J.G., and SIDDHARTHAN, R.V. (1993), *On the characteristics of nonlinear soil response* Bulletin of the Seismological Society of America, 83, 218–244.
- ZEGHAL, M., ELGAMAL, A., TANG, H., and STEPP, J. (1995), *Lotung Downhole Array. II: Evaluation of Soil Nonlinear Properties*, J. Geotech. Engrg., 121(4), 363–378.